Electronic Supplementary Material (ESI) for Journal of Materials Chemistry A.

Supplementary Information

$LaFeO_3$ meets nitrogen-doped graphene functionalized with ultralow Pt loading in an impactful Z-scheme flatform for photocatalytic hydrogen evolution

Dung Van Dao[a,b], Giovanni Di Liberto[c], Hyungduk Ko[d], Jaehong Park[b], Wenmeng Wang[b], Doyeong Shin[b], Hoki Son[b], Quyet Van Le[b], Tuan Van Nguyen[e], Vo Van Tan[f], Gianfranco Pacchioni[c,*] and In-Hwan Lee[b,*]

---

[a] *Institute of Research and Development, Duy Tan University, Da Nang 550000, Vietnam*
[b] *Department of Materials Science and Engineering, Korea University, Seoul 02841, Republic of Korea*. E-mail: *ihlee@korea.ac.kr*
[c] *Dipartimento di Scienza dei Materiali, Università degli Studi di Milano-Bicocca, Via Roberto Cozzi 55, Milano 20125, Italy. E-mail: gianfranco.pacchioni@unimib.it*
[d] *Nanophotonics Research Center, Korea Institute of Science and Technology, Seoul 02792, Korea*
[e] *School of Chemical Engineering and Materials Science, Chung-Ang University, Seoul 02841, Republic of Korea*
[f] *Department of Chemistry, University of Education, Hue University, Hue 530000, Vietnam*

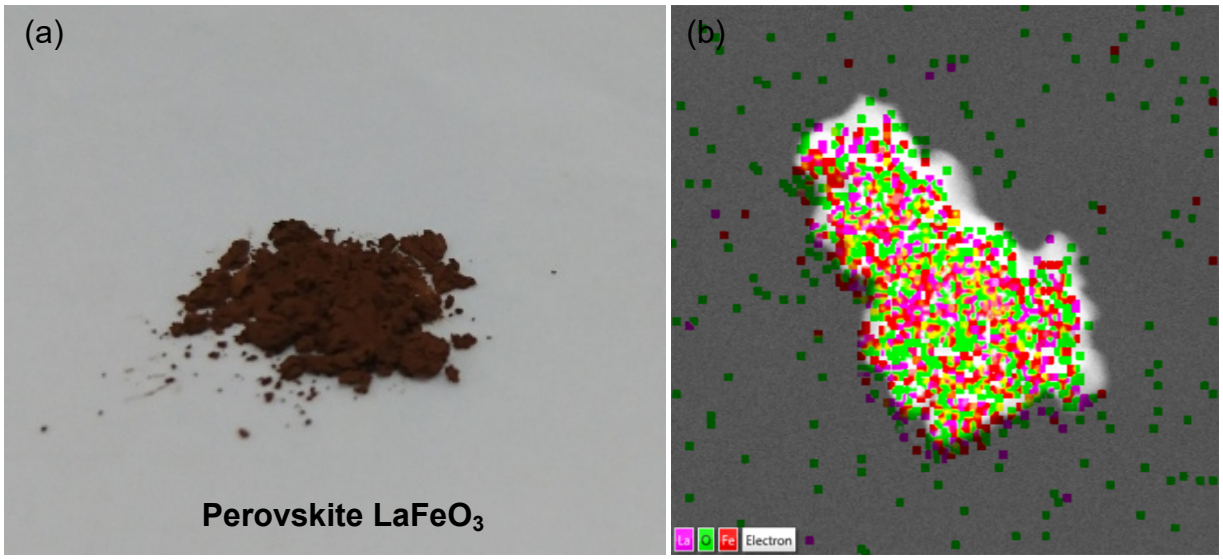

Fig. S1 (a) Photographs of as-prepared $LaFeO_3$ and (b) their merged TEM elemental map.

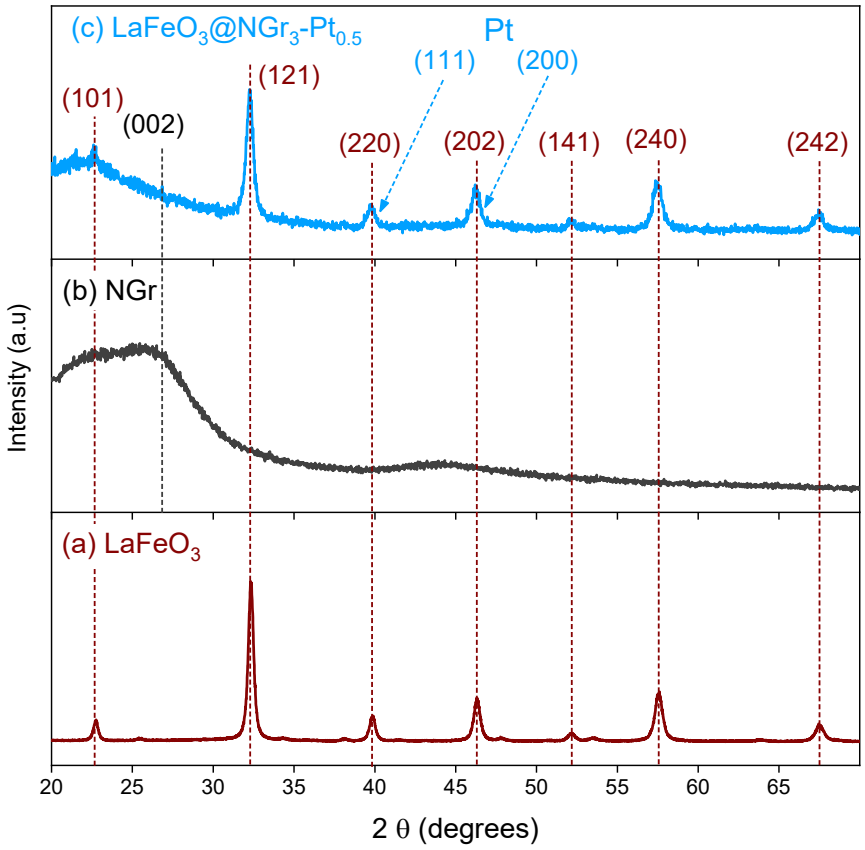

Fig. S2. XRD pattern measurement of as-prepared free-standing (a) $LaFeO_3$, (b) NGr, and (c) $LaFeO_3$@NGr_3-$Pt_{0.5}$ materials.

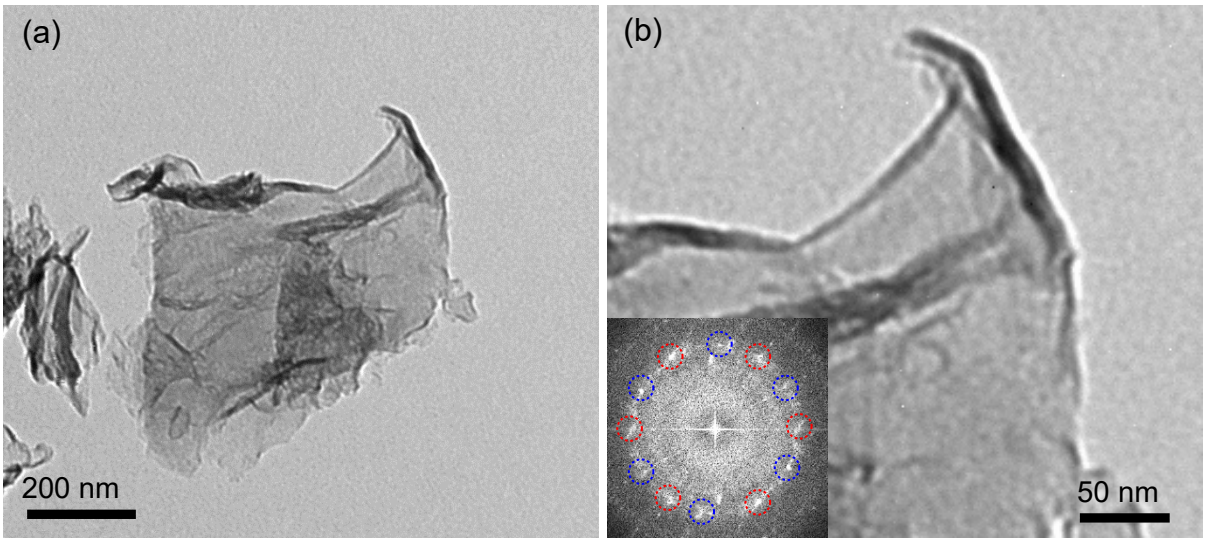

Fig. S3 (a and b) TEM image of free-standing NGr sample, and the SEAD of as-obtained NGr given in the inset of b panel.

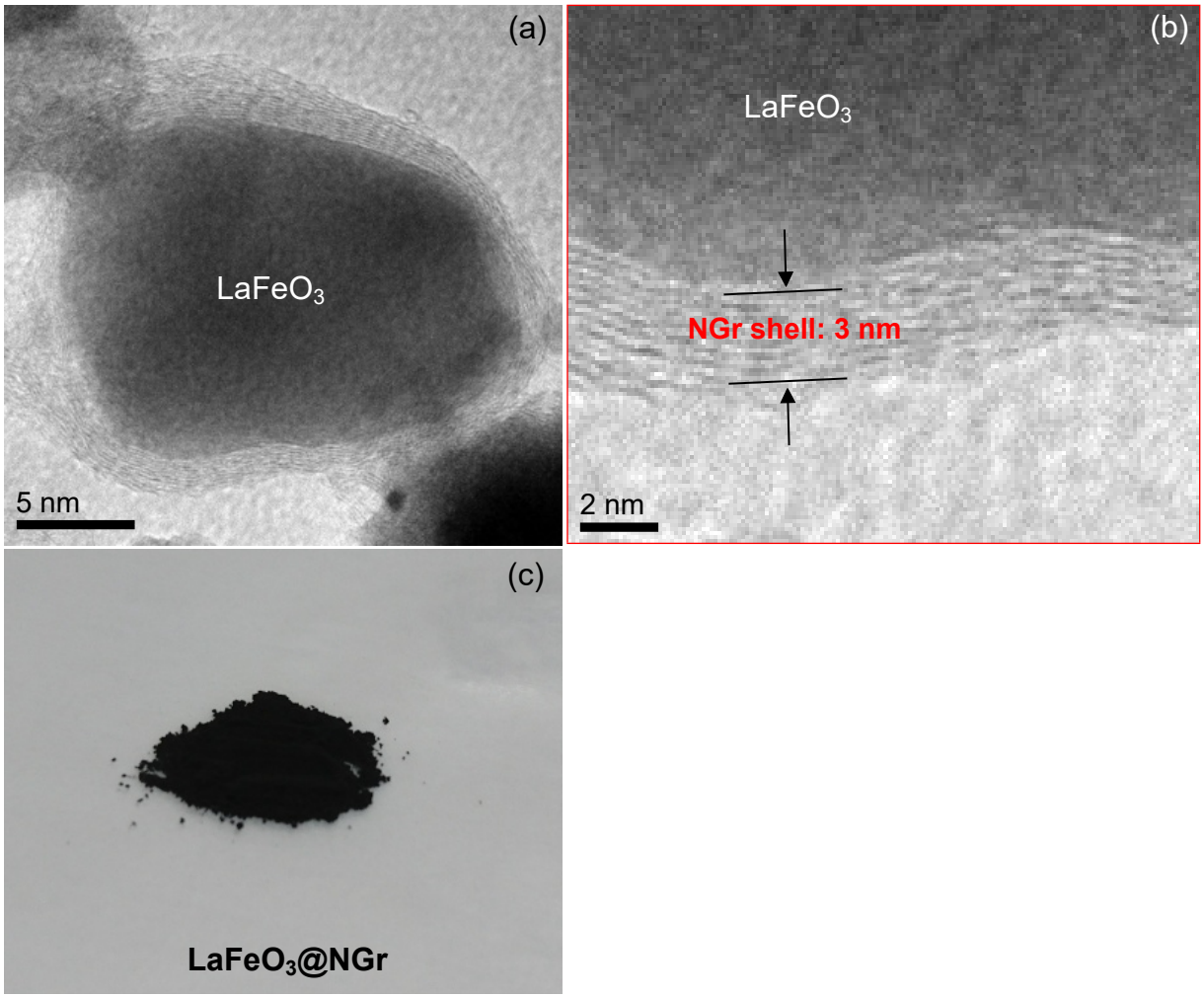

Fig. S4. TEM image of as-pyrolyzed $LaFeO_3$@NGr_3 with a clean surface of NGr shell, where the NGr shell thickness is approximately 3 nm. (c) Photographs of as-prepared $LaFeO_3$@NGr_3 black powders.

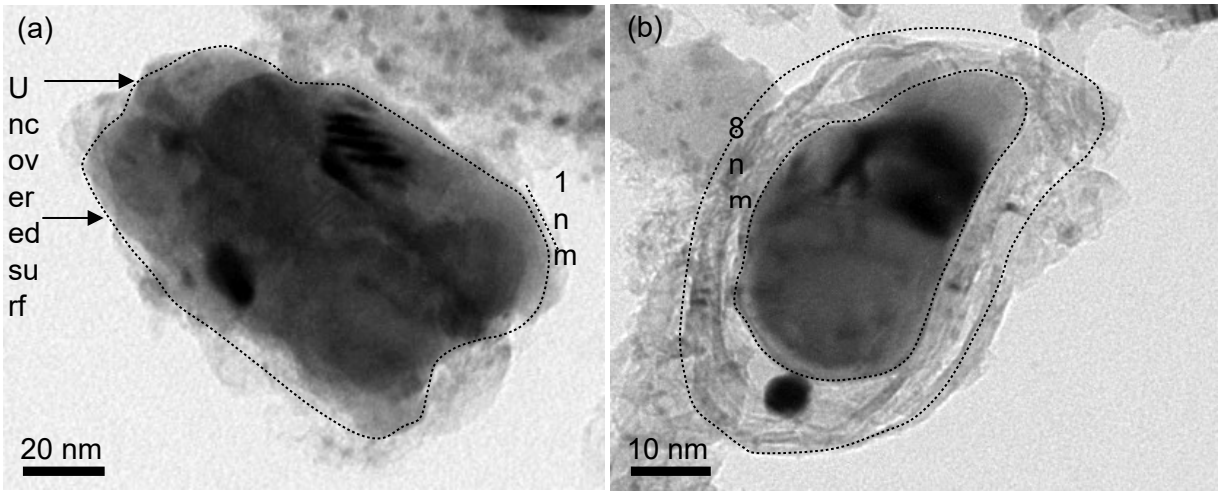

Fig. S5 TEM image of as-pyrolyzed (a) $LaFeO_3$@NGr_1 with NGr shell thickness of 1 nm and (b) $LaFeO_3$@NGr_8 with NGr shell thickness of 8 nm.

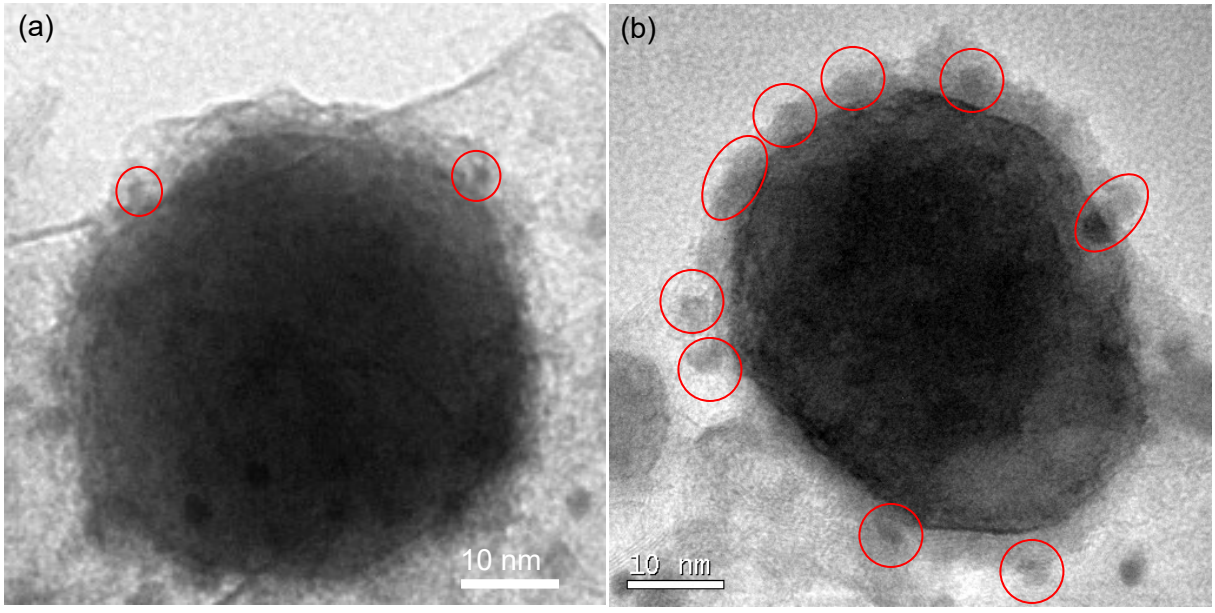

Fig. S6 TEM image of (a) $LaFeO_3$@NGr_3-$Pt_{0.2}$ and (b) $LaFeO_3$@NGr_3-$Pt_{2.0}$ samples, where the attached Pt NPs are indicated by the red circles.

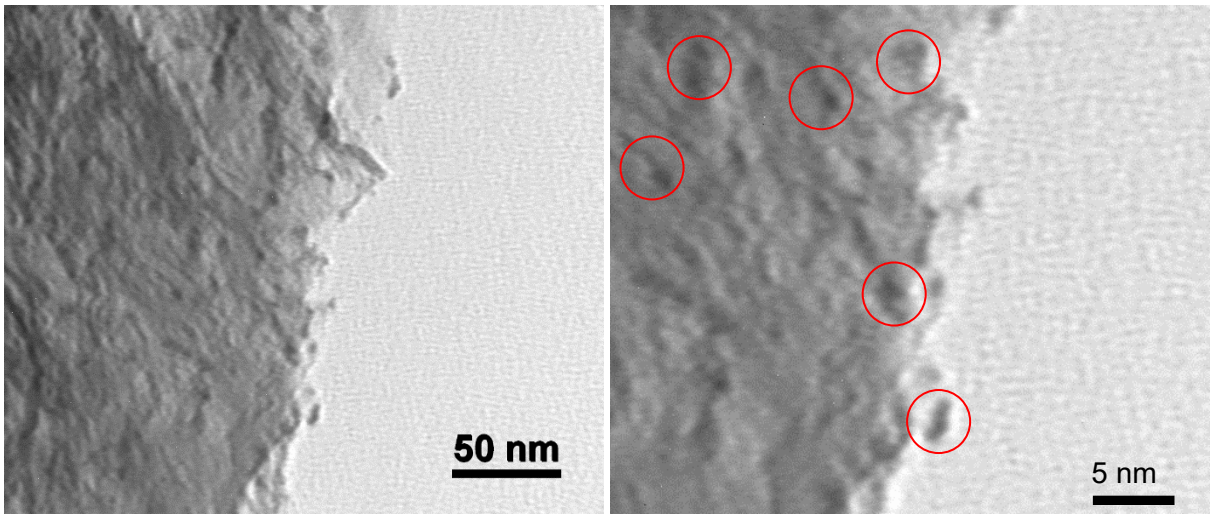

Fig. S7 TEM image of NGr-$Pt_{0.5}$ sample, where the attached Pt NPs are indicated by the red circles with an average size of 3 nm.

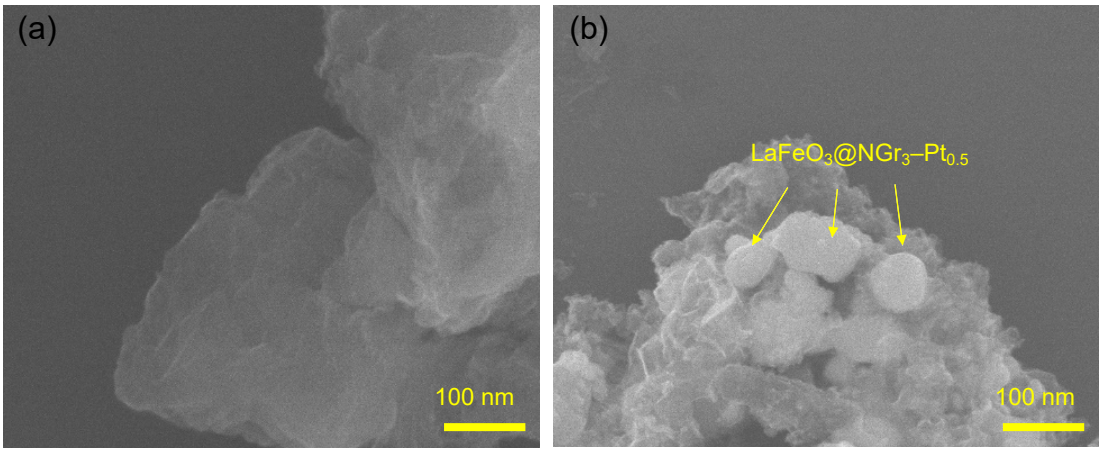

Fig. S8 FESEM observation for (a) free-standing NGr and (b) $LaFeO_3$@NGr_3–$Pt_{0.5}$ hybrids.

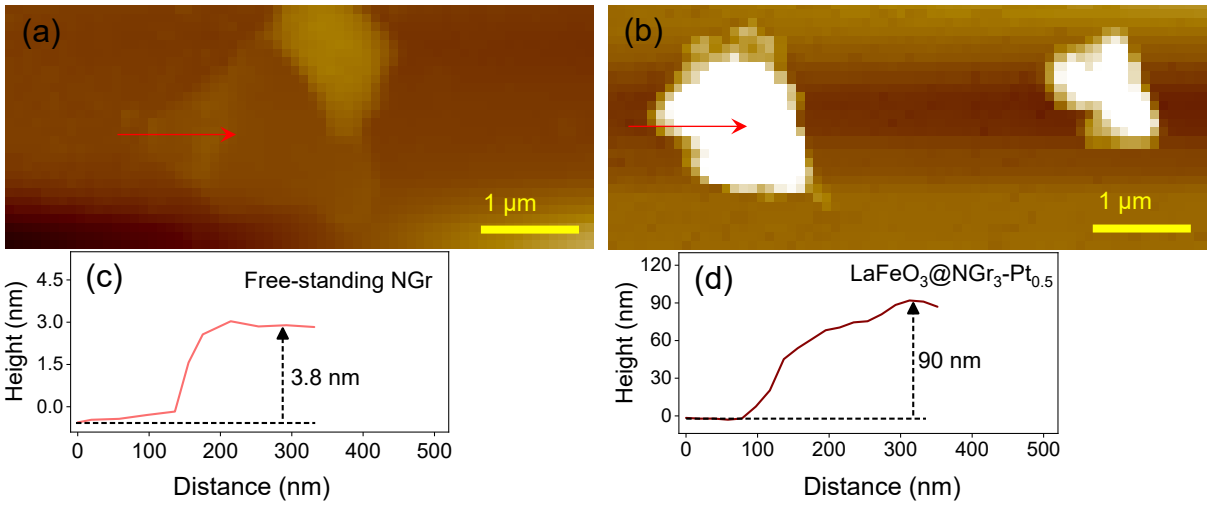

Fig. S9 AFM images and corresponding height profiles of (a, c) free-standing NGr and (b, d) $LaFeO_3$@NGr_3–$Pt_{0.5}$ hybrid.

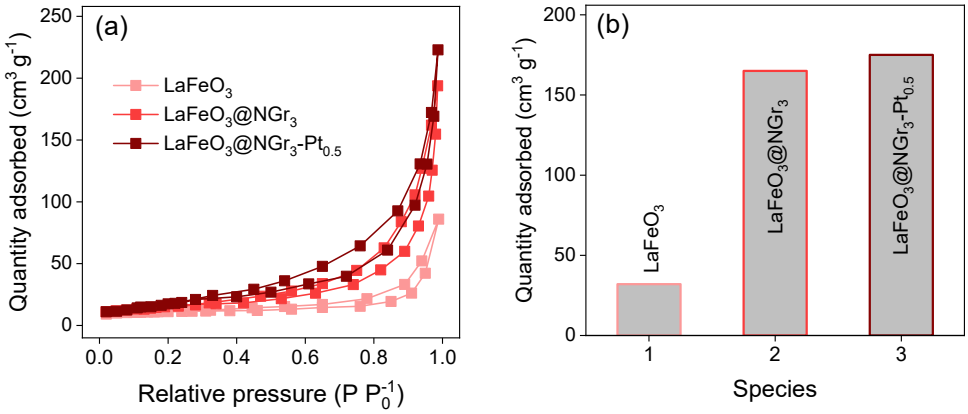

Fig. S10 (a) Nitrogen adsorption/desorption isotherms and (b) corresponding BET surface areas for free-standing $LaFeO_3$, $LaFeO_3$@NGr_3, and $LaFeO_3$@NGr_3–$Pt_{0.5}$ hybrid photocatalysts.

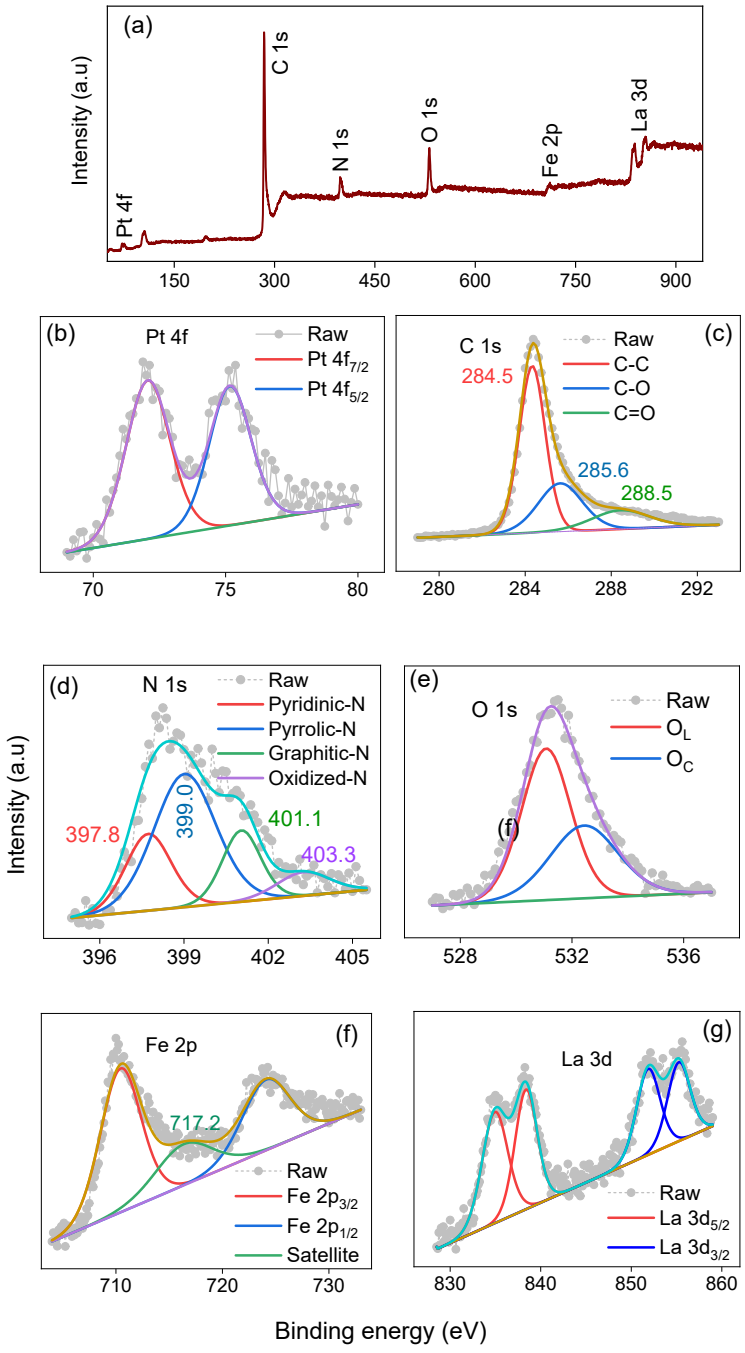

Fig. S11 XPS-measured results for $LaFeO_3$@NGr_3–$Pt_{0.5}$ hybrid: (a) full survey for all ingredients and their corresponding high-resolution analysis of (b) Pt 4f, (c) C 1s, (d) N 1s, (e) O 1s, (f) Fe 2p, and (g) La 3d, respectively.

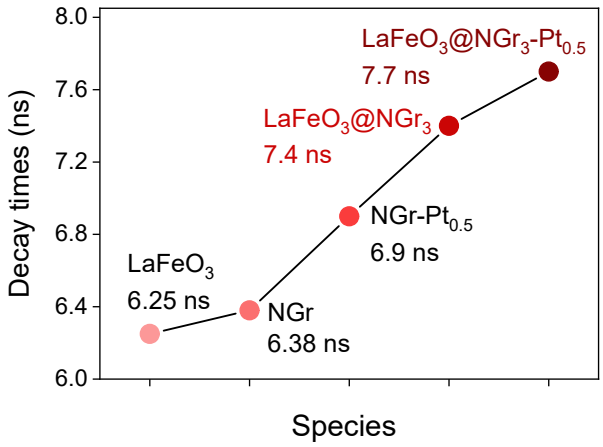

Fig. S12 Their corresponding decay times for free-standing $LaFeO_3$ and NGr, NGr–$Pt_{0.5}$, $LaFeO_3$@NGr_3, and $LaFeO_3$@NGr_3–$Pt_{0.5}$ hybrids, respectively.

DFT Calculations

Independent $LaFeO_3$ and NGr units

We fully optimized the bulk structure of orthorhombic $LaFeO_3$, starting from the experimental crystal lattice.[1] The calculated *a*, *b*, and *c* lattice vectors are 5.521 Å, 5.541 Å, and 7.782 Å respectively. They compare well with the available experimental ones, with deviations as high as 1%. The magnetic ordering of atomic spins resembles the overall anti-ferromagnetic behavior of the material, where the atomic magnetization of each Fe site is $\pm 4.17\ \mu_B$, comparable with the measured one ($\pm 4.6\ \mu_B$), and with previous reports at the same level of theory ($\pm 4.2\ \mu_B$).[2–4] The computed band gap at the PBE+U level (2.63 eV) is close to the experimental one,[3] while at the HSE06 level is overestimated by about 1 eV (3.59 eV).[3] This result can be understood in light of the magnetic insulator nature of this oxide, where more elaborated approaches are needed to provide reliable band gap estimates.[5]

The bulk structure has been used to construct the (010) crystal surface. The atomic coordinates where fully relaxed at fixed slab cell. This surface is stable, non-polar, often highly-exposed.[4] All these properties are important when modelling interfaces.[6] In addition, it shows an acceptable lattice mismatch with the graphene nanosheets (see below). We modelled a ~2 nm thick (010) surface, which guarantees converged surface properties. The *a* and *b* lattice parameters are 5.521 Å, and 7.782 Å. The calculated surface energy is 1.03 Jm^{-2} at the level of PBE+U, similar to previous reports (1.02 Jm^{-2}).[4] A similar value is obtained at HSE06 level (1.10 Jm^{-2}). If dispersion forces are included, the surface energy increases to 1.45 Jm^{-2}. The band gap at HSE06 level (3.48 eV) is almost the same of the bulk phase, indicating the absence of surface states.

The computed lattice parameters of a graphene single layer are: $a = b = 3.275$ Å, $g = 120°$. We modelled a rotated supercell containing 48 atoms, and we added 4 Nitrogen atoms with a pyridinic, pyrrolic, and graphitic arrangement, as observed experimentally. The lattice vectors *a*, *b*, and *g* of the rotated supercell are 9.824 Å, 12.750 Å, and 90°. The addition of N atom

results into a sizeable band gap of the system, 1.94 eV at HSE06 level, close to that measured experimentally (2.1 eV). The structure of both $LaFeO_3$ (010) and NGr are reported in **Fig. S11**.

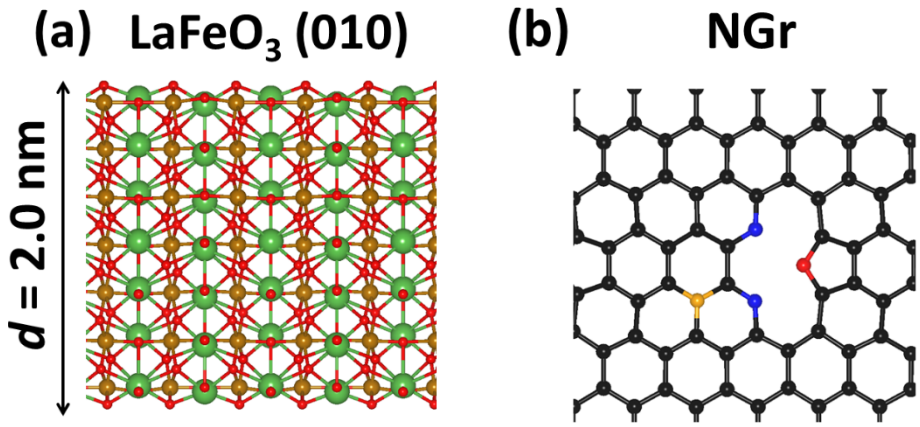

Fig. S13 (a) Side view of $LaFeO_3$ (010). La: Green; Fe: light brown; O: red. (b) NGr sheet, where different N atoms indicated by different colours: pyridinic N: blue; pyrrolic N: red: graphitic N: orange. The atoms coordination is similar to previous reports.[7,8]

$LaFeO_3$@NGr interface

The NGr film has been rotated to form the interface with the $LaFeO_3$ (010) surface to avoid spurious effects due to strain.[9] In particular, we fixed the lattice vectors at those of $LaFeO_3$ (010) and we released the strain to the NGr part. The resulting mismatch is 2.9%, 5.6% and 0.0% for *a*, *b* and g lattice parameters, respectively.

The N-dopant concentration is roughly twice that measured experimentally, to keep the simulation cell at a reasonable size. Figure S1 shows the optimized interface which is a classical van de Waals heterojunction, as confirmed also by the calculated adhesion energy (-0.3 Jm^{-2}).

We calculated the band offsets by using the line-up methodology based on the core energy levels (1s orbitals) as a reference.[10–13] This methodology, at variance with the approach based

on the electrostatic potential, can be adopted when simulating thin films and/or 2D materials.[14] This strategy is widely adopted also in XPS studies.[15–17] The Valance Band Offset (*VBO*) of the interface is calculated by aligning the Valence Band Maximum (*VBM*) of the separated components (VBM_1, VBM_2) with respect to the core energy levels evaluated in both heterojunction ($E_{1,1s}^{Het}$, $E_{2,1s}^{Het}$) and separated units ($E_{1,1s}$, $E_{2,1s}$) as reported in Eq. S1.

$$VBO = \left(VBM_1 - E_{1,1s}\right) - \left(VBM_2 - E_{2,1s}\right) + \left(E_{1,1s}^{Het} - E_{2,s}^{Het}\right) \quad \text{Eq. S1}$$

Then the Conduction Band Offset (*CBO*) can be obtained by including the band gap of the materials. HSE06 functional well reproduces the electronic structure of NGr, while it overestimates the band gap of $LaFeO_3$. For this reason, we adopt the strategy followed in other works where the *CBO* is calculated by using the experimental band gap.[18,19] The calculated *VBO* and *CBO* are 0.74 eV, and 0.44 eV, quite close to the measured ones, 0.63 eV and 0.39 eV. The difference between the two is within the typical range of accuracy of band alignment methodologies.[20,21] The band edges of NGr are higher in energy than those of $LaFeO_3$ indicating a type-II alignment.

We then evaluated the role of interface polarization, since it may drive the charge separation from classical type-II heterostructures to Direct Z-scheme ones.[22–25] The impact of interface polarization has been evaluated by looking at the interface dipole of the heterojunction, which is -0.6 *D*, where the negative sign indicates a charge accumulation on the $LaFeO_3$ side, and consequent depletion on the NGr side. This result is corroborated by the analysis of the charge density different (D*r*) averaged along the non-periodic direction (<Dr_z>).[26,27] Both analyses lead to the same conclusion. The interface polarization causes a bending of the band edges at the interface consistent with a Direct Z-scheme behavior.[22] Upon excitation electrons will accumulate on NGr, and holes on $LaFeO_3$.

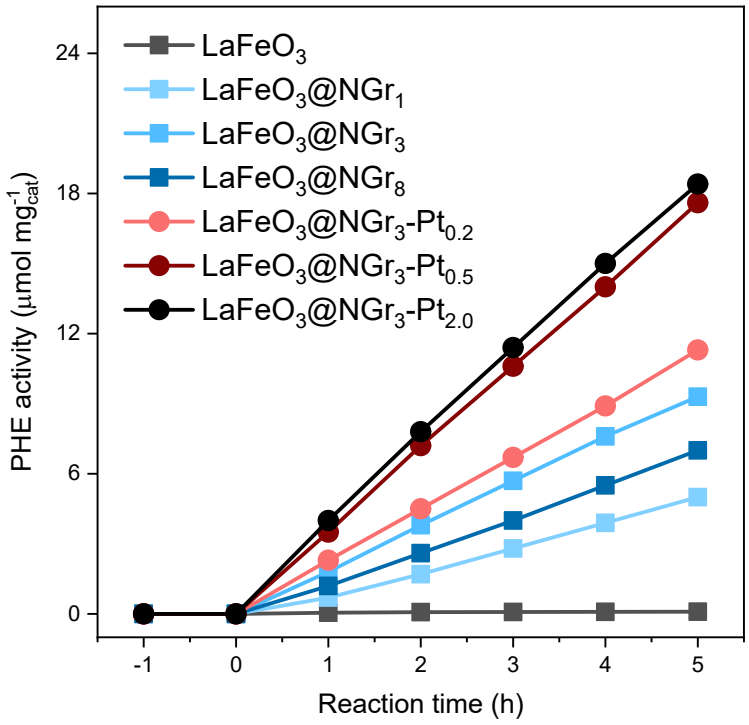

Fig. S14 PHE activity over free-standing $LaFeO_3$, $LaFeO_3$@NGr_x with different NGr shell thickness of 1, 3, and 8 nm, and $LaFeO_3$@NGr_3–Pt_y with different Pt cocatalyst loading of 0.2, 0.5, and 2.0 wt%.

References

1 M. Marezio and P. D. Dernier, *Mater. Res. Bull.*, 1971, **6**, 23–29.

2 W. C. Koehler and E. O. Wollan, *J. Phys. Chem. Solids*, 1957, **2**, 100–106.

3 A. M. Ritzmann, A. B. Muñoz-García, M. Pavone, J. A. Keith and E. A. Carter, *Chem. Mater.*, 2013, **25**, 3011–3019.

4 I. W. Boateng, R. Tia, E. Adei, N. Y. Dzade, C. R. A. Catlow and N. H. de Leeuw, *Phys. Chem. Chem. Phys.*, 2017, **19**, 7399–7409.

5 L. A. Cipriano, G. Di Liberto, S. Tosoni and G. Pacchioni, *J. Chem. Theory Comput.*, 2020, acs.jctc.0c00134.

6 E. Cerrato, C. Gionco, M. C. Paganini, E. Giamello, E. Albanese and G. Pacchioni, *ACS Appl. Energy Mater.*, 2018, **1**, 4247–4260.

7 Q. Tang, Z. Zhou and Z. Chen, *Nanoscale*, 2013, **5**, 4541.

8 X.-F. Li, K.-Y. Lian, L. Liu, Y. Wu, Q. Qiu, J. Jiang, M. Deng and Y. Luo, *Sci. Rep.*, 2016, **6**, 23495.

9 G. Di Liberto, L. A. Cipriano, S. Tosoni and G. Pacchioni, *Chem. – A Eur. J.*, 2021, chem.202101764.

10 S.-H. Wei and A. Zunger, *Appl. Phys. Lett.*, 1998, **72**, 2011–2013.

11 G. Di Liberto, S. Tosoni and G. Pacchioni, *ChemCatChem*, 2020, **12**, 2097–2105.

12 G. Di Liberto, S. Tosoni, F. Illas and G. Pacchioni, *J. Chem. Phys.*, 2020, **152**, 184704.

13 D. O. Scanlon, C. W. Dunnill, J. Buckeridge, S. A. Shevlin, A. J. Logsdail, S. M. Woodley, C. R. A. Catlow, M. J. Powell, R. G. Palgrave, I. P. Parkin, G. W. Watson, T. W. Keal, P. Sherwood, A. Walsh and A. A. Sokol, *Nat. Mater.*, 2013, **12**, 798–801.

14 L. A. Cipriano, G. Di Liberto, S. Tosoni and G. Pacchioni, *J. Phys. Chem. C*, 2021, **125**, 11620–11627.

15 R. W. Grant, E. A. Kraut, S. P. Kowalczyk and J. R. Waldrop, *J. Vac. Sci. Technol. B Microelectron. Process. Phenom.*, 1983, **1**, 320–327.

16 J. R. Waldrop, S. P. Kowalczyk, R. W. Grant, E. A. Kraut and D. L. Miller, *J. Vac. Sci. Technol.*,

1981, **19**, 573–575.

17 E. A. Kraut, R. W. Grant, J. R. Waldrop and S. P. Kowalczyk, *Phys. Rev. B*, 1983, **28**, 1965–1977.

18 N. R. D'Amico, G. Cantele and D. Ninno, *Appl. Phys. Lett.*, 2012, **101**, 141606.

19 S. A. Chambers, T. Ohsawa, C. M. Wang, I. Lyubinetsky and J. E. Jaffe, *Surf. Sci.*, 2009, **603**, 771–780.

20 K. Steiner, W. Chen and A. Pasquarello, *Phys. Rev. B*, 2014, **89**, 205309.

21 G. Di Liberto and G. Pacchioni, *J. Phys. Condens. Matter*, 2021, **33**, 415002.

22 Q. Xu, L. Zhang, J. Yu, S. Wageh, A. A. Al-Ghamdi and M. Jaroniec, *Mater. Today*, 2018, **21**, 1042–1063.

23 J. Low, J. Yu, M. Jaroniec, S. Wageh and A. A. Al-Ghamdi, *Adv. Mater.*, , DOI:10.1002/adma.201601694.

24 J. Low, C. Jiang, B. Cheng, S. Wageh, A. A. Al-Ghamdi and J. Yu, *Small Methods*, 2017, **1**, 1700080.

25 C. Miranda, H. Mansilla, J. Yáñez, S. Obregón and G. Colón, *J. Photochem. Photobiol. A Chem.*, 2013, **253**, 16–21.

26 J. Liu, *J. Phys. Chem. C*, 2015, **119**, 28417–28423.

27 J. Liu and E. Hua, *J. Phys. Chem. C*, 2017, **121**, 25827–25835.